Acta Materialia 199 (2020) 495–503

Contents lists available at ScienceDirect

Acta Materialia

journal homepage: www.elsevier.com/locate/actamat

Full length article

Shear-strain-induced over 90° rotation of local magnetization in FeCoSiB/PMN-PT (011) multiferroic heterostructures

Xinger Zhao[a,1], Ren-Ci Peng[a,1], Zhongqiang Hu[a,*], Tiannan Yang[b], Weixiao Hou[a], Yuqing Zhou[c], Tao Li[c], Qin Du[a], Yuxin Cheng[a], Jingen Wu[a], Zhiguang Wang[a], Ziyao Zhou[a], Long-Qing Chen[b], Ming Liu[a,*]

[a] Electronic Materials Research Laboratory, Key Laboratory of the Ministry of Education & International Center for Dielectric Research, School of Electronic Science and Engineering, State Key Laboratory for Mechanical Behavior of Materials, Xi'an Jiaotong University, Xi'an 710049, China
[b] Department of Materials Science and Engineering, Penn State University, University Park, PA, 19019, USA
[c] Center for Spintronics and Quantum System, State Key Laboratory for Mechanical Behavior of Materials, School of Materials Science and Engineering, Xi'an Jiaotong University, Xi'an, Shaanxi 710049, China

ARTICLE INFO

Article history:
Received 12 March 2020
Revised 8 August 2020
Accepted 19 August 2020
Available online 26 August 2020

Keywords:
Magnetoelectric effect
Shear strain
Magnetic domain
Magneto-optical Kerr effect

ABSTRACT

Strain-mediated magnetoelectric effect can be utilized as an energy-efficient approach for spin manipulation. However, over 90° magnetization rotation is still challenging in un-patterned magnetic films, as the piezo-strain driven by ferroelectric domain switching is generally uniaxial rather than unidirectional, which limits the developments of non-volatile magnetic memory and logic devices. Here we demonstrate the rotation of local magnetization with a large angle of 136° by applying strains with a shear component at a fixed magnetic field of 45 Oe in FeCoSiB/PMN-PT (011) multiferroic heterostructures, revealed by a vector-resolved quantitative magneto-optical Kerr effect (MOKE) microscopy. Phase-field simulations confirm that the approximate 140° rotation of magnetization vectors is a consequence of the shear strain associated with ferroelectric/ferroelastic switching of PMN-PT (011) substrates. The visualization of over 90° magnetization rotation induced by the strain with a shear component paves the way for deterministic magnetization switching that has important implications in the energy-efficient spintronic devices.

1. Introduction

Magnetic domain dynamics in thin films are of great importance for the potential applications in magnetic memory and logic devices [1,2]. Magnetic field and spin-polarized current have been the conventional driving forces to switch the magnetic domains [3–7]. However, both methods require a large electric current with high power consumption, which limits the development of high-density spintronic devices. Therefore, promising energy-efficient alternatives that are employing electric fields instead of currents to modulate spin and magnetic domain dynamics have been proposed. In ferromagnetic metal/metal-oxide heterostructures such as Co/GdO_x and Co/AlO_x, the applied electric fields can manipulate the magnetic anisotropy, thereby controlling the magnetic domain wall motion via charge accumulation, activation energy barrier modulation, or oxygen migration [8–11]. Besides, ionic liquid gating could be utilized to regulate the evolution of magnetic domains [12]. Electric fields induced strain- or charge-mediated manipulation of magnetic domains has also been demonstrated in ferromagnetic/ferroelectric multiferroic heterostructures [13–18].

Among the interaction mechanisms for electric field control of magnetism in magnetoelectric heterostructures [19–24], due to the flexibility of selections for materials with large magnetoelectric coupling coefficients [25], the strain-mediated magnetoelectric coupling effect has attracted more attention. However, due to the uniaxial strains caused by electric fields, it has been challenging to achieve over 90° magnetization rotation, unless the multilayers are designed with strong shape anisotropy [22,26,27] or unidirectional exchange coupling [28]. Recently, a shear strain effect has been first utilized to control the evolution of magnetic domains in Ni/PMN-PT (011) multiferroic heterostructures, where rotation angles of 62-84° rather than the hitherto expected 90° were observed by high-resolution vector maps of magnetization with the pixel-by-pixel comparison [29].

In this work, we demonstrate the rotation of local magnetization with a large angle of 136° by applying strains with a shear component at 45 Oe in FeCoSiB/PMN-PT (011) multiferroic

* Corresponding authors.
E-mail addresses: zhongqianghu@xjtu.edu.cn (Z. Hu), mingliu@xjtu.edu.cn (M. Liu).
[1] These authors contributed equally to this work.

https://doi.org/10.1016/j.actamat.2020.08.041
1359-6454/

heterostructures, revealed by vector-resolved quantitative MOKE microscopy. Meanwhile, phase-field simulations unravel an approximate 140° rotation of magnetic domains mediated by electric-field-induced ferroelectric/ferroelastic switching strain from the PMN-PT (011) substrates, which are consistent with the experimental results. The direct observation of the shear-strain-mediated magnetization rotation over 90° would be a significant step for deterministic magnetization switching that has potential applications in energy-efficient spintronics such as magnetic memory and logic devices.

2. Experimental details

2.1. Sample preparation

The Cu(3 nm)/ FeCoSiB(44 nm)/Ta(3 nm) multilayers were deposited on PMN-PT (011) piezoelectric single crystals via dc magnetron sputtering at room temperature. For each preparation of samples, the base pressure was below 1.5×10^{-7} Torr, and working dc power was fixed at 30W. The top Cu capping layer was prepared to protect FeCoSiB magnetic layer from oxidation. The commercial PMN-PT (011) substrates were 0.5 mm thick. In addition, the back of the substrate was covered with a 20 nm Ta layer as a bottom electrode.

2.2. Experiment characterization

In-situ measurements of electric field regulation of magnetism were executed at room temperature. Vector-resolved quantitative MOKE microscope (Evico Magnetics, em-Kerr-Highres) in longitudinal MOKE mode with a 4-pole horizontal magnet was utilized for the real-time visualization of magnetic domain evolution under in-situ magnetic fields as well as electric fields. A commercial software for the MOKE system was used to analyze the specific magnetization directions of magnetic domains, and the deviation of the acquired magnetization directions was less than 5° [30]. The magnetization directions were obtained by substituting magnetic domain patterns in two orthogonal sensitivity directions measured at the same time into the calibration functions, which were calculated according to the Kerr contrast of the single domains under saturated magnetic fields in different directions [30]. Before applying the electric field to the piezoelectric substrate, a magnetic field of 300 Oe was applied along the [100] direction and then decreased to -45 Oe, and during the electrical modulation process, the magnetic field remained unchanged at -45 Oe. The polarization versus electric field (P-E) hysteresis loop was measured via a commercial precision ferroelectric tester and ferroelectric domains were imaged by Piezoresponse Force Microscopy (PFM). Magnetic hysteresis loops were measured by VSM (Lake Shore 7404) and MOKE. FMR spectra were recorded with the aid of the ESR system (JEOL, JES-FA200), working at TE 011 mode at approximately 9.2 GHz. Additionally, electric fields were applied making use of a Keithley 6517B Electrometer.

2.3. Phase-field model

In the phase-field model, the temporal evolution of the local magnetization vector M can be described by the Landau–Lifshitz–Gilbert equation:

$$\left(1+\alpha^2\right)\frac{\partial \mathbf{M}}{\partial t} = -\gamma_0(\mathbf{M}\times\mathbf{H}_{\text{eff}}) - \frac{\gamma_0\alpha}{M_s}\mathbf{M}\times(\mathbf{M}\times\mathbf{H}_{\text{eff}}) \quad (1)$$

where α and γ_0 denote the Gilbert damping coefficient and the gyromagnetic ratio, respectively. Eq. (1) can be solved using a semi-implicit Fourier spectral method [31] with a small-time step Δt of about 0.09 ps. The effective magnetic field is expressed by $\mathbf{H}_{\text{eff}} = -(1/\mu_0)(\delta F_{\text{tot}}/\delta \mathbf{M})$, where μ_0 represents the vacuum permeability; F_{tot} is the total magnetic free energy of the amorphous FeCoSiB film, expressed as,

$$F_{\text{tot}} = \int_V (f_{\text{ms}} + f_{\text{exch}} + f_{\text{external}} + f_{\text{uni,anis}} + f_{\text{elastic}} + f_{\text{mc}})dV \quad (2)$$

where f_{ms}, f_{exch}, f_{external}, $f_{\text{uni, anis}}$, f_{elastic} and f_{mc} are magnetostatic, exchange, external magnetic field (i.e., arising from $H_{[100]}$=-45 Oe), the initial uniaxial anisotropy along the [01-1] direction, elastic, and magnetocrystalline anisotropy energy densities, respectively. Among them, magnetocrystalline anisotropy energy density (f_{mc}) is neglected in the simulation because of the isotropic nature of the amorphous FeCoSiB film. The periodic magnetostatic boundary condition is employed in the phase-field simulations. The mathematical expressions and numerical solutions of the f_{ms}, f_{exch}, f_{external}, $f_{\text{uni, anis}}$ and f_{elastic} can be found in the literature [32].

Three-dimensional grids of $150\Delta x \times 150\Delta y \times 36\Delta z$ with real grid sizes of Δx=Δy= 3 nm and Δz=2 nm are utilized to describe the bottom substrate layer (=$10\Delta z$), its overlaying FeCoSiB film layer (=$22\Delta z$) and the top air layer (=$4\Delta z$). The simulated dimension for FeCoSiB film is 450 nm × 450 nm × 44 nm. The material parameters of FeCoSiB film utilized for the simulations are listed as follows: the saturated magnetization M_s=1.01092×10^6 A/m [33]; elastic constants c_{11}= 201.92 GPa, c_{12}= 86.54 GPa, c_{44}= 57.69 GPa [34,35]; saturation magnetostriction λ_s= -25 ppm (ref. λ_s= -5 ppm (metal-glass, amorphous) [36]; Gilbert damping coefficient α= 0.06 [33]; gyromagnetic ratio γ_0=1.76×10^{11} $\text{T}^{-1}\text{s}^{-1}$ [37]; and exchange constant A_{ex}= 1.7×10^{-11} J/m [37].

3. Results and discussion

3.1. Characterization of basic properties

To investigate shear-strain-mediated magnetoelectric effect, Cu(3 nm)/FeCoSiB(44 nm)/Ta(3 nm)/PMN-PT (011) multiferroic heterostructures were prepared via magnetron sputtering. The measurement configuration for the FeCoSiB/PMN-PT (011) multilayers is shown in Fig. 1a, in which electric fields are applied across the PMN-PT (011) substrates and the yellow arrows indicate the direction of the positive electric fields. The FeCoSiB/PMN-PT (011) multiferroic heterostructures exhibit in-plane anisotropy, as illustrated in Fig. 1b. Derived from the magnetic hysteresis loops measured by MOKE, the in-plane easy axis lies in the [01-1] direction of the piezoelectric substrates, and the in-plane hard axis is along the [100] direction.

The magnetization directions of magnetic domains are calculated by a commercial software based on the Kerr contrast change of the domain patterns (see *Experimental Section*) [30]. Due to the complex distribution of the magnetization directions, angles from 0° to 360° are utilized to unravel the relative orientation of domains, and the corresponding color wheel and scale bar of magnetic domain patterns are shown in the left of Fig. 1c. When the samples are saturated by positive and negative magnetic fields along the [100] direction, the corresponding magnetization directions of magnetic domains are defined as 0° and 180°, respectively. With magnetic fields lying in the [01-1] direction, the magnetization directions under positive and negative saturated magnetic fields are set as 90° and 270°, respectively. Additionally, the angles rotate counterclockwise. The crystal orientation of the PMN-PT (011) substrates with respect to the angles around the color wheel are also displayed in the left of Fig. 1c.

The dynamic magnetization reversal along the in-plane hard axis (i.e., magnetic fields in the [100] direction) is shown in Fig. 1c. The magnetic domains of FeCoSiB are clearer with more regular shape, and the magnetic domain variations are better defined.

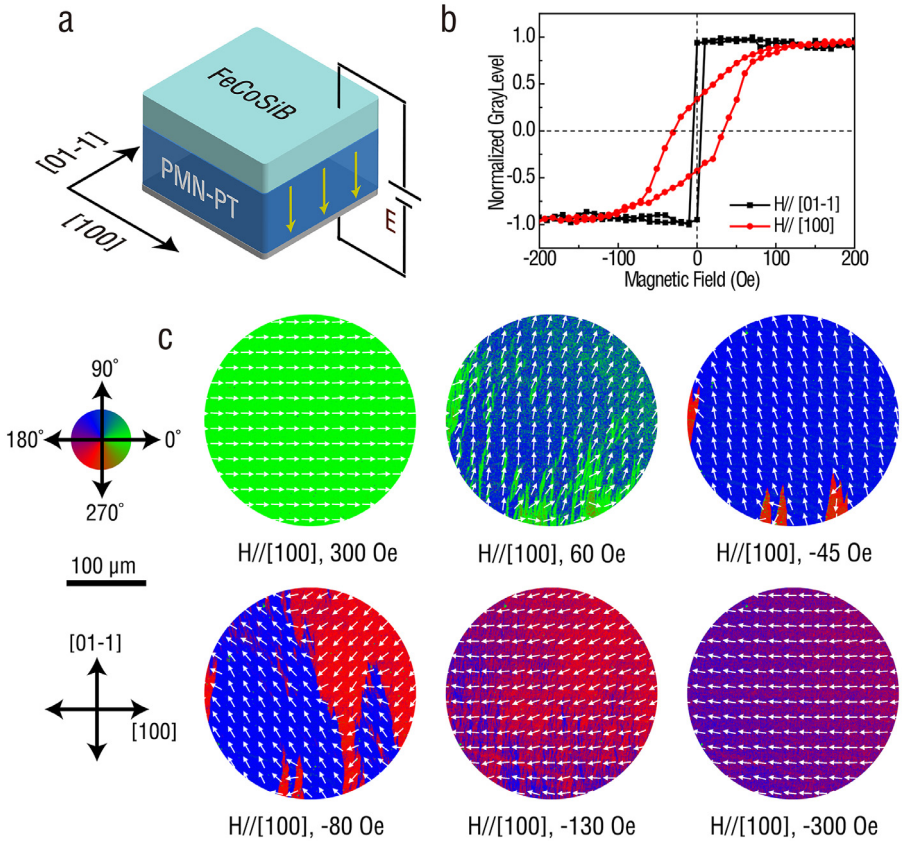

Fig. 1. Structure of multiferroic heterostructures and characterization of basic magnetic properties. (a) Schematic of FeCoSiB/PMN-PT (011) heterostructures. (b) In-plane magnetic hysteresis loops with magnetic fields along [01-1] (black line) and [100] directions (red line), respectively. (c) Evolution of magnetic domains during a magnetization cycle with magnetic fields in the [100] direction. (For interepretation of the references to color in this figure legend, the reader is referred to the web version of this article.)

With the magnetic fields decrease from 300 Oe to 0 Oe, the magnetization directions of magnetic domains gradually rotate from 0° to nearly 90°. As the magnetic fields continue decreasing, magnetic domains with 225° magnetization directions nucleate from the top-right corner and gradually expand with domain wall propagation. At a magnetic field of -300 Oe, the magnetic domains rotate to 180° uniformly, leading to a single domain state with the magnetization direction lying along the direction of the magnetic field. For the in-plane easy axis along [01-1], the magnetization switching process can be found in Fig. S1.

Fig. 2a displays the P-E hysteresis loop of PMN-PT single crystals. The used rhombohedral PMN-PT (011) single crystal substrates have four structural domains (r1, r2, r3, r4) where r1 and r2 mean polarization along the out-of-plane direction, and r3 as well as r4, refers to the polarization lying in the in-plane direction [38]. As mentioned in previous work [29,39], when the electric field near the coercive field of PMN-PT (011) substrates was applied, the polarization of PMN-PT (011) underwent 71° ferroelastic switching from $r1^+$ to $r3^+$ or $r4^-$ and 109° ferroelastic switching from $r1^+$ to $r3^-$ or $r4^+$ and 180° ferroelectric switching from $r1^+$ to $r1^-$, as illustrated in Fig. 2b. Form our early work, both 71° and 109° ferroelastic switching cover up 90% of the entire poled area from the peak intensity analysis of reciprocal space mapping [39]. Fig. 2c displays the schematic of the linear and shear strain effects. The linear strain is directly proportional to the applied field. However, the shear strain effect is different, which is characterized by a shear strain in the (011) plane accompanied with a normal strain along the [01-1] direction, when the polarization of the PMN-PT (011) substrates undergoes 71° and 109° ferroelastic switching from the out-of-plane to the in-plane direction with an electric field equal to the coercive field of the piezoelectric substrates [29,40]. To induce an in-situ linear strain effect, the heterostructures are initially polarized by a positive electric field that is much larger than the coercive field of the PMN-PT (011) substrates, and in the subsequent regulation process, the polarity of the electric fields is maintained. In contrast, to induce the shear strain effect, electric fields with opposite polarity are applied. To image the ferroelectric domains, out-of-plane PFM phase and amplitude images under different poling voltages are shown in Fig. 2d-e. A two-step 71° and 109° ferroelastic switching makes the polarizations rotate from the downward direction into the in-plane direction, and subsequently to the upward direction. In the poled area marked by blue dashed lines, all polarization vectors point downwards under the applied voltage as +5 V. When a negative voltage of -2 V is applied on the tip, the polarization vectors rotate to an intermediate state with most along the in-plane direction, and with the decrease of the voltage to -6 V, all of the polarizations point upwards. The two-step 71° and 109° ferroelastic switching between in-plane and out-of-plane directions are utilized to provide the shear strain effect within size comparable to that of many micro MEMS devices. Because the selected region (approximately 50 μm) is much larger than the ferroelectric domains, the differences of magnetic responses to various ferroelectric domains can be ignored.

3.2. Linear strain effect mediated magnetoelectric effect

Fig. 3a shows the in-situ magnetic domain evolution induced by the linear strain effect. A multi-domain region is taken as the initial state at -45 Oe along the [100] direction due to the relatively simple magnetization distribution, which is suitable for the

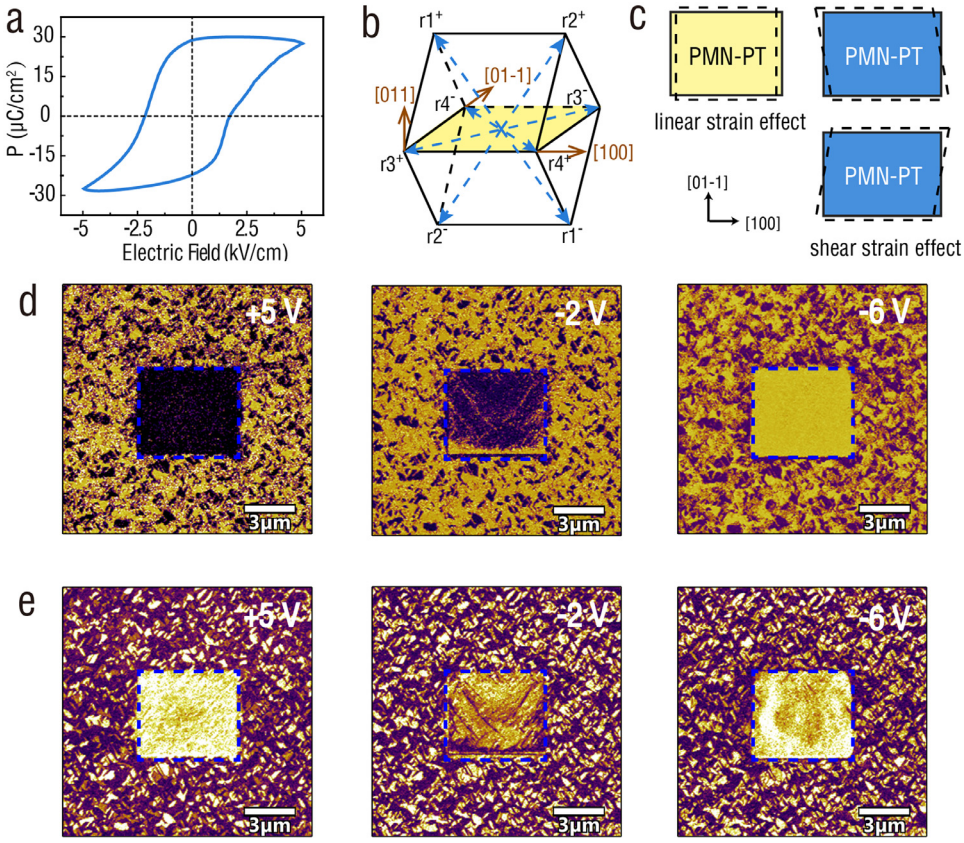

Fig. 2. Ferroelectric properties of PMN-PT(011) single crystals. (a) P-E loop. (b) Schematic of possible domain switching routes. (c) Schematic of the linear and shear strain effects. (d) The out-of-plane PFM phase images with electrically poled regions in the square area marked by the blue dashed lines. (e) The corresponding PFM amplitude images after being poled by different voltages. (For interepretation of the references to color in this figure legend, the reader is referred to the web version of this article.)

analysis of the magnetic response to the electric fields, as shown in Fig. 1c. This magnetic field remains constant during the strain modulation process. The magnetic domain patterns remain stable for over 10 min at 0 kV/cm, suggesting that the change of the magnetization direction would only be caused by the strain-mediated magnetoelectric effect rather than the magnetic field or the environmental disturbance. As the electric field increases to 3 kV/cm, 225° magnetic domains cover nearly half of the view. At 4 kV/cm, the electric field drives the 225° magnetic domains to occupy the vast majority of the field of view. Under the linear strain effect, magnetic domains gradually propagate with the sequential increase in the electric fields. The corresponding video of the magnetization rotation process under the linear strain effect can be found in Video S1 in the Supporting Information. Fig. 3b shows the hysteresis loops along [100] under the linear strain effect, measured by a vibrating sample magnetometer (VSM). With the increase in electric fields, the initial hard axis becomes easier for magnetizing. The normalized magnetization values (M/M_s) are extracted from the hysteresis loops and displayed in Fig. 3c, showing an expected linear relationship between the magnetization and the electric fields at both 0 Oe and -45 Oe.

3.3. Shear strain effect mediated magnetoelectric effect

Fig. 4a illustrates the evolution of magnetic domains under the shear strain effect with a magnetic field of -45 Oe along [100] within the same area of Fig. 3, right after the removal of the electric field of +5 kV/cm. When the negative electric field decreases from -1 to -1.8 kV/cm, the rotation angle of magnetization direction is more than 90° in some area, corresponding to the nonlinear strain effect introduced by 71° and 109° ferroelastic switching near the negative electric coercive field of the piezoelectric PMN-PT (011) single crystals. According to the previous reports [29], it was found that when an electric field near the coercive field was applied to drive the polarization to switch into the in-plane direction (the (011) plane) through 71° and 109° ferroelastic switching, the rhombohedral PMN–PT substrates would induce a normal strain along the [01-1] direction and more importantly, a shear strain within the (011) plane. This shear strain effect was also found in rhombohedral PZN-PT [40], but hitherto it has been rarely mentioned. In order to eliminate the interference of residual ferroelectric domains to the magnetic vector analysis, MOKE image at an electric field of -1.8 kV/cm is displayed, which is slightly larger than the coercive field. Additionally, when the electric field continuously decreases to -4 kV/cm, magnetic domain patterns remain mostly unchanged. In other words, compared with that magnetic domains vary gradually with the increase of electric fields under the linear strain effect, the shear strain effect induces the orientation of magnetic domains to change abruptly at the coercive field of the ferroelectric substrates and the rotation of magnetization directions over 90° in some local areas. The corresponding MOKE video is shown as Video S2 in the Supporting Information.

To clearly reveal that the shear strain effect can drive magnetic domains changing over 90° at -45 Oe, magnetic domain patterns marked by gray lines in Fig. 4a are magnified as illustrated. At 0 kV/cm, the magnetization directions of magnetic domains are in 224.3°, and at -1 kV/cm, the magnetization directions are parallel to 222.1°. When electric fields are sequentially decreased to -1.8 kV/cm, the shear strain effect drives the magnetization directions to change to 85.7°. It means that electric fields drive the magnetization directions of magnetic domains to change 136.4° exceeding 90° under the shear strain effect. As electric fields reduced to

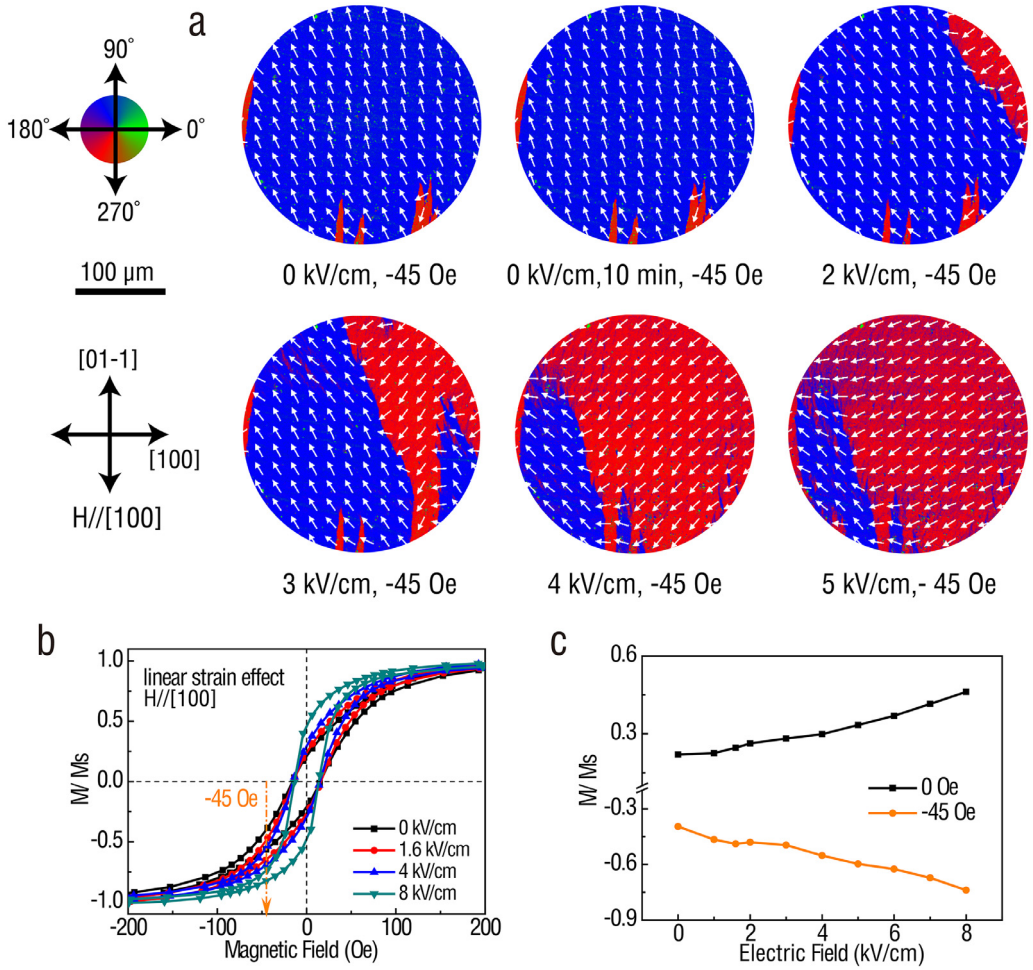

Fig. 3. Linear strain effect mediated magnetoelectric effect. (a) The response of magnetic domains to the electric fields. During the tests, a small magnetic field (-45 Oe) parallel to [100] is maintained. (b) Hysteresis loops at different electric fields with magnetic fields along [100]. (c) Normalized magnetization value (M/M_s) as a function of electric fields at 0 Oe (black line) and -45 Oe (orange line), respectively. (For interepretation of the references to color in this figure legend, the reader is referred to the web version of this article.)

-4 kV/cm, the magnetization directions remain approximately unchanged along 82.7°. Pixel-by-pixel comparison of the shear strain effect induced magnetic domain variation between -1 kV/cm and -1.8 kV/cm is illustrated in Fig. S2, where most of the variation angles are located around 140° (orange regions), and the size of the switching area is larger than 30 × 30 μm^2.

The reversibility and reproducibility of the shear strain effect induced over 90° rotation of local magnetization are clarified as shown in Fig. S3. With the magnetic field of -45 Oe unchanged, when the applied electric fields change to the opposite direction (positive electric fields), the shear strain effect induced over 90° rotation of local magnetization can be observed again. The rotation direction of magnetic domains changing more than 90° under positive electric fields is opposite to that under negative electric fields, which facilitates magnetic domains approximately restore after a polarization cycle.

Electric field control of hysteresis loops under the shear strain effect by VSM can be seen in Fig. 4b. Like under the linear strain effect modulation, the multiferroic heterostructures become easier for magnetizing along the initially hard axis direction under the shear strain effect. More clearly, the normalized magnetization values extracted from hysteresis loops are displayed in Fig. 4c as a function of the absolute values of electric fields. The normalized magnetization values under the linear strain effect are approximately linearly related to the electric fields, but a sudden increase of it emerges at the coercive field of the substrates under the shear strain effect, that is, the maximum modulation of the values is acquired at the coercive field rather than larger electric fields.

Fig. 4 illustrates that several snapshots of magnetic domains for the marked area within a size range of about 50 μm are uniform, but the switching dynamic processes of magnetic domains within 50 μm are non-uniform and incoherent because of both the dominant magnetostatic energy (rather than exchange energy) and the heterogeneous strain of ferroelastic polarization switching as seen by the previous report [41]. The equilibrium magnetic domains experimentally observed are uniform, which is possibly because the local uniform ferroeletric domain of PMN-PT after dynamic polarization switching induced a relatively uniform strain region. It is worth to be further studied in the future.

At the same time, to demonstrate the credibility of the displayed magnetic domain patterns under the shear strain effect modulation, the variation of magnetic domains with magnetic fields after the third test is exhibited in Fig. 5. The magnetic fields are continuously reduced along the same direction based on the original applied magnetic field as -45 Oe. Like the dynamic magnetization process with magnetic fields along the [100] direction shown in Fig. 1c, the switching of magnetic domains is also composed of domain wall motion and domain rotation. With the decrease of magnetic fields, magnetic domains whose magnetization directions are approximately 90° are diminished with the expan-

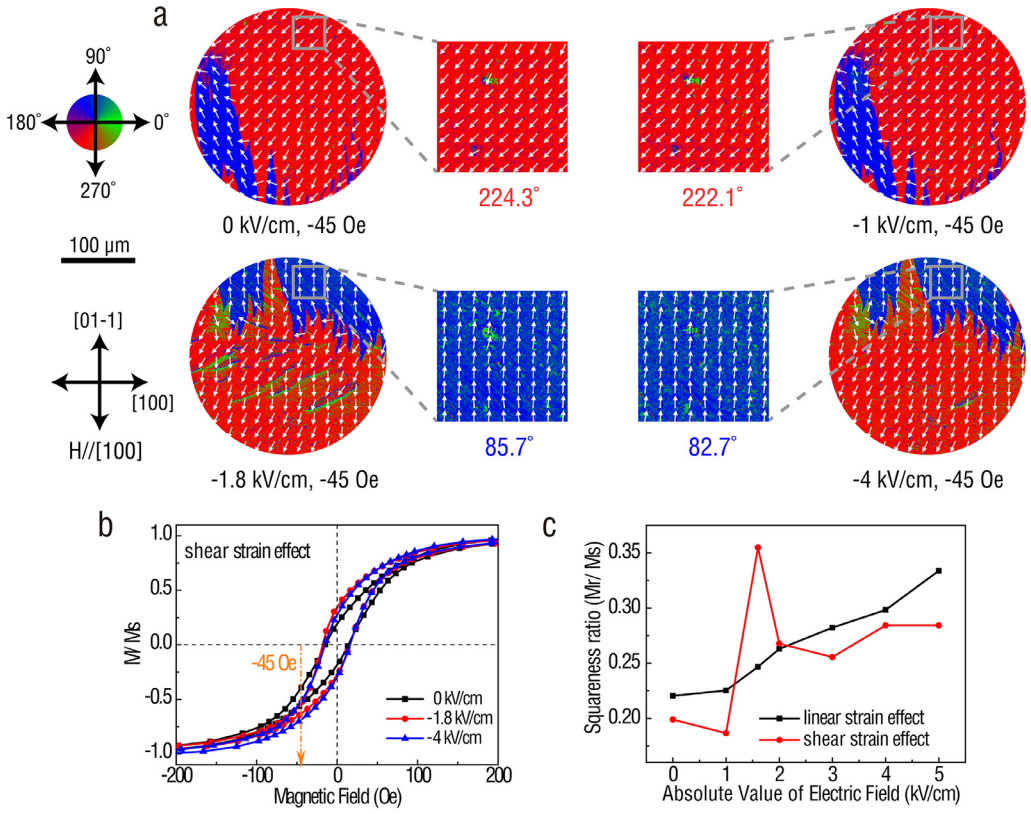

Fig. 4. Shear strain effect mediated magnetoelectric effect. (a) Electric-field-driven magnetic domain evolution under the shear strain effect. Magnified images of the marked area by gray lines show a large rotation angle of the local magnetization over 90°. (b) Hysteresis loops at different electric fields with magnetic fields along [100]. (c) Normalized magnetization values as a function of the absolute values of electric fields.

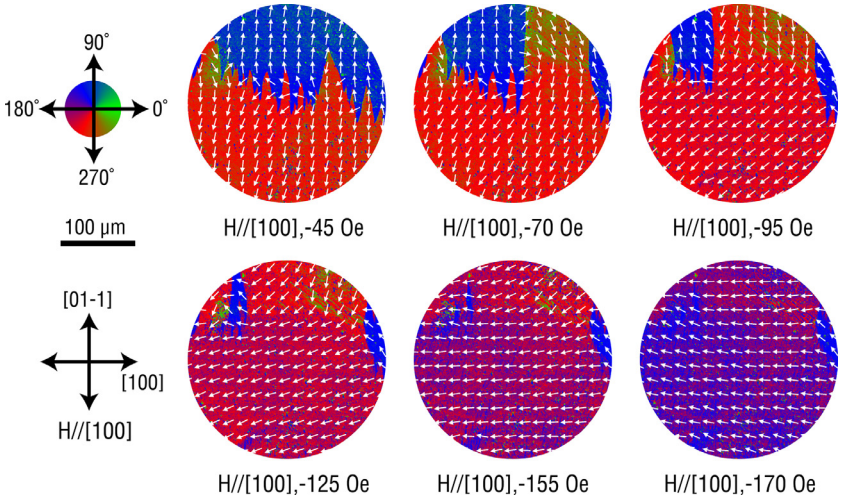

Fig. 5. The response of magnetic domains to magnetic fields after applying the shear strain effect. These images are taken in the same area as in Fig. 4, but after releasing the sample from -5 kV/cm, showing recovery of local magnetization by magnetic fields.

sion of magnetic domains in other directions, and the magnetization directions of magnetic domains in a large area gradually rotate to 180° (the magnetic field direction).

3.4. Phase-field simulations of electric field control of magnetic domains

In order to further reveal the electric field control of magnetic domains, phase-field simulations were performed during ferroelectric polarization switching of PMN-PT (011) substrates. There exists an initial anisotropy along the [01-1] direction from the magnetic hysteresis loops in Fig. 1b, and it is hard to directly obtain the value of the uniaxial anisotropy (K_{anis}) or anisotropy field (H_{ani}) from Fig. 1b. Hence, a K_{anis} ($=H_{anis}M_s=75$ Oe $\times$ 1.01092 $\times$ 10^6 A/m$=7581.9$ J/m^3) along [01-1] was assumed during the simulation. Fig. 6a shows the initial state of a magnetic single-domain at zero electric fields, which is obtained by the synergistic effect of K_{anis} and the external magnetic field $H_{[100]}=$ -45 Oe. When an electric field of +5 kV/cm is applied to the PMN-PT (011), the polarization aligns downward, and it provides a linear anisotropic

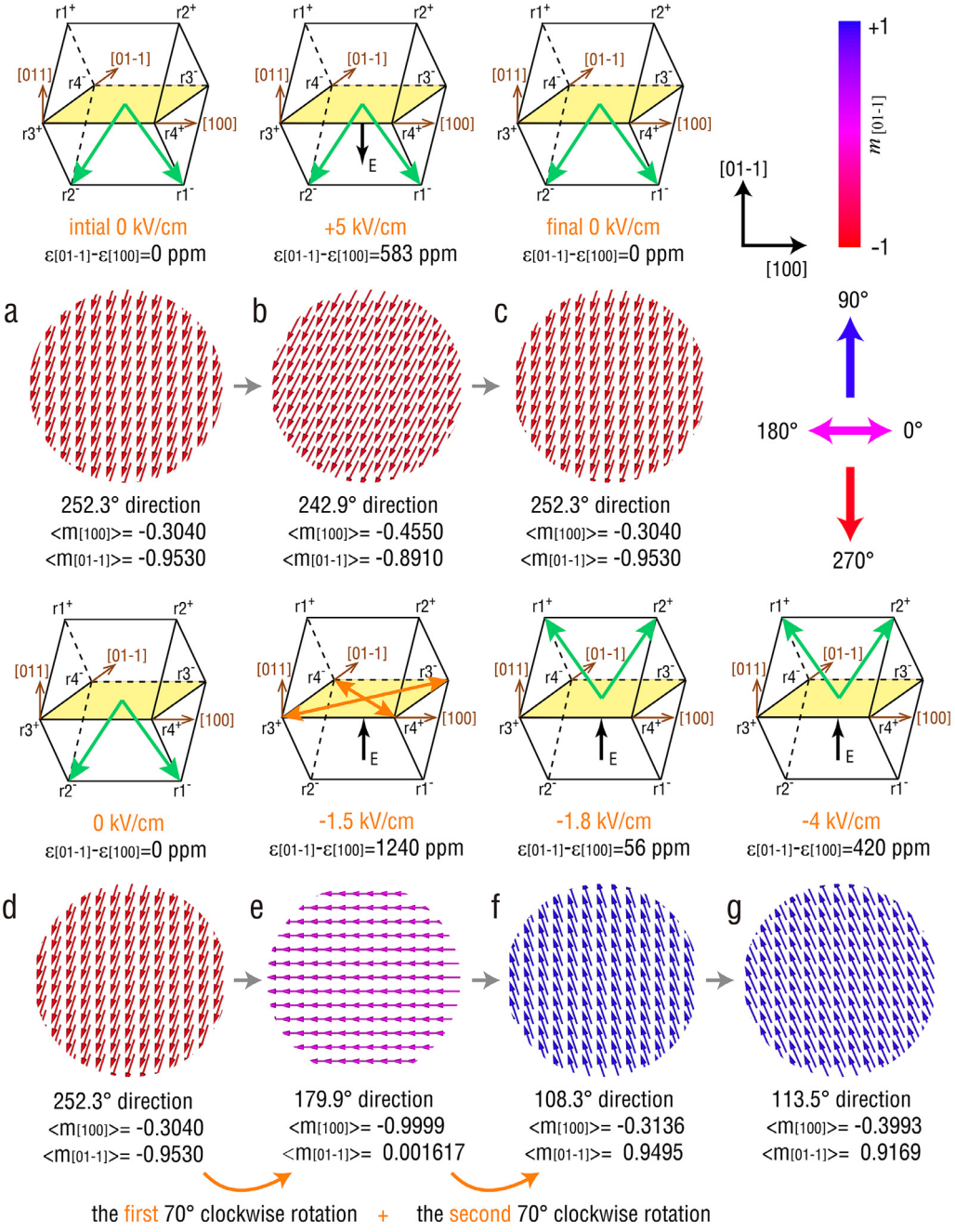

Fig. 6. Ferroelectric domain switching and distribution of the magnetization vectors at different electric fields under the corresponding ferroelectric/ferroelastic strains via phase-field simulations. The magnetic domain patterns and the average magnetization components ($<m_{[100]}>$ and $<m_{[01-1]}>$) under (a-c) the linear strain effect and (d-g) the shear strain effect, respectively. The arrows represent the orientations of local magnetization vectors in (a-g), where magnetization directions along the [100] and [-100] directions are defined as 0° and 180°, and that in the [01-1] and [0-11] directions are set as 90° and 270°.

piezo-strain of $\varepsilon_{[01\text{-}1]}$-$\varepsilon_{[100]}$ = 583 ppm [42,43]. Due to the negative magnetostriction coefficient of the FeCoSiB film, the magnetization direction rotates to [-100] slightly under the linear strain-induced magnetoelastic anisotropy shown in Fig. 6b. After removing the positive electric fields, the linear strain disappears, and the magnetic domain state almost returns to the initial state, as illustrated in Fig. 6c.

Then, electric fields with the opposite polarity, that is, negative electric fields are applied to PMN-PT (011) piezoelectric substrates. Fig. 6d shows the magnetization distribution at 0 kV/cm. When the applied negative electric field approached the coercive field of PMN-PT (011) (E_c=-1.5 kV/cm), the out-of-plane polarization state becomes the metastable in-plane polarization state by 71° or 109° ferroelastic switching, generating a large ferroelastic strain of $\varepsilon_{[01\text{-}1]}$-$\varepsilon_{[100]}$ = 1240 ppm [42]. Fig. 6e reveals the corresponding metastable magnetic single domain whose magnetization direction is along [-100], that is, the magnetization direction is switched clockwise by 70° approximately under the large ferroelastic nonlinear strain-induced magnetoelastic anisotropy. Once the applied electric field exceeds the coercive field, another ferroelastic switching from the in-plane polarization state to the opposite out-of-plane polarization state occurs, and then the large ferroelastic nonlinear strain disappears. The magnetization direction is switched clockwise by 70° approximately again via magnetization

precession because of the positive average component of magnetization (e.g., $<m_{[01\text{-}1]}> = 0.0016 > 0$) with the synergistic effect of K_{anis} and the external magnetic field $H_{[100]}$= -45 Oe, as shown in Fig. 6f. In other words, under the shear strain effect, it can be realized that electric fields induced the magnetization rotation greater than 90° (i.e., approximately 140°) by the two-step switching of the magnetization directions of magnetic domains. It is well evidenced by the rotation of local magnetization over 90° (i.e., approximately 136.4°) observed in the experimental results of the shear strain effect control. The 140° instead of the expected 90° rotation of magnetic domains may be caused by the combination of the shear strain effect and the application of a magnetic field along [100]. When the negative electric field is decreased to -4 kV/cm in Fig. 6g, the magnetization direction of magnetic domains rotates slightly to [-100] compared to that at -1.8 kV/cm. Furthermore, the simulation of magnetic domain evolution with the shear strains switched off can be found in Fig. S4, where the magnetization vectors rotate clockwise by 37.5° rather than to the [-100] direction.

Here, magnetization rotation greater than 90° through the two-step magnetization switching mediated by electric-field-induced ferroelastic-strain is not deterministic. It is mainly attributed to the second-step magnetization switching, which depends on magnetization precession after ferroelastic polarization switching to the out-of-plane direction when the electric field is larger than the coercive field. Once the time for ferroelastic polarization switching is controlled precisely, the local magnetization rotation greater than 90° will be deterministic. Furthermore, the simulation could be found in Fig. S5 for $<m_{[01\text{-}1]}>$ that has a small negative component.

It is illustrated in Fig. S6 that the variation of ferromagnetic resonance (FMR) fields with electric fields measured by in-situ electron spin resonance (ESR) when magnetic fields are in the [100] direction. The linear strain effect induces FMR fields to gradually move to the lower magnetic fields with the sequential increase of electric fields, but under the shear strain effect, the maximum tunability of FMR fields is acquired at electric fields near the coercive field of the PMN-PT (011) substrates. Furthermore, the electric field regulation of hysteresis loops and FMR fields with magnetic fields along the [01-1] direction is presented in Fig. S7, and Fig. S8, respectively.

4. Conclusion

In summary, direct visualization of the magnetic domain evolution induced by the linear strain effect and the shear strain effect has been demonstrated in FeCoSiB/PMN-PT (011) multiferroic heterostructures utilizing quantitative MOKE microscopy. Under the linear strain effect, magnetic domains gradually expanded with electric fields. In contrast, under the shear strain effect, the orientation of magnetic domains changed abruptly at the ferroelectric coercive field of the PMN-PT (011) substrates and then remained even if the absolute value of electric fields kept increasing. It was observed that the rotation of local magnetization could be as high as 136° induced by the shear-strain-mediated magnetoelectric effect, which was further confirmed by phase-field simulations. The direct visualization of electric fields induced magnetic domain propagation is significant for the applications of multiferroic heterostructures in low power spintronic devices such as magnetic memory and logic devices.

Declaration of Competing Interest

The authors declare that they have no known competing financial interests or personal relationships that could have appeared to influence the work reported in this paper.

Acknowledgments

This work was supported by the National Key R&D Program of China (grant no. 2018YFB0407601), the Natural Science Foundation of China (grant nos. 91964109, 51802248, 11534015, 51902247 and 51802250), the National 111 Project of China (B14040), and Basic Research Program of Natural Science of Shaanxi Province (grant no. 2020JQ-059).

Supplementary materials

Supplementary material associated with this article can be found, in the online version, at doi:10.1016/j.actamat.2020.08.041.

References

[1] S.S.P. Parkin, M. Hayashi, L. Thomas, Magnetic domain-wall racetrack memory, Science 320 (2008) 190–194.
[2] D.A. Allwood, G. Xiong, C.C. Faulkner, D. Atkinson, D. Petit, R.P. Cowburn, Magnetic domain-wall logic, Science 309 (2005) 1688–1692.
[3] J. Shibata, G. Tatara, H. Kohno, A brief review of field- and current-driven domain-wall motion, J. Phys. D: Appl. Phys. 44 (2011) 1384004.
[4] G.S.D. Beach, C. Nistor, C. Knutson, M. Tsoi, J.L. Erskine, Dynamics of field--driven domain-wall propagation in ferromagnetic nanowires, Nat. Mater. 4 (2005) 741–744.
[5] M. Hayashi, L. Thomas, Y.B. Bazaliy, C. Rettner, R. Moriya, X. Jiang, S.S.P. Parkin, Influence of current on field-driven domain wall motion in permalloy nanowires from time resolved measurements of anisotropic magnetoresistance, Phys. Rev. Lett. 96 (2006) 197207.
[6] T.A. Moore, I.M. Miron, G. Gaudin, G. Serret, S. Auffret, B. Rodmacq, A. Schuhl, S. Pizzini, J. Vogel, M. Bonfim, High domain wall velocities induced by current in ultrathin Pt/Co/AlOx wires with perpendicular magnetic anisotropy, Appl. Phys. Lett. 93 (2008) 262504.
[7] M.X. Wang, W.L. Cai, K.H. Cao, J.Q. Zhou, J. Wrona, S.Z. Peng, H.W. Yang, J.Q. Wei, W. Kang, Y.G. Zhang, J. Langer, B. Ocker, A. Fert, W.S. Zhao, Current-induced magnetization switching in atom-thick tungsten engineered perpendicular magnetic tunnel junctions with large tunnel magnetoresistance, Nat. Commun. 9 (2018) 671.
[8] U. Bauer, S. Emori, G.S.D. Beach, Electric field control of domain wall propagation in Pt/Co/GdOx films, Appl. Phys. Lett. 100 (2012) 192408.
[9] A.J. Schellekens, A. van den Brink, J.H. Franken, H.J.M. Swagten, B. Koopmans, Electric-field control of domain wall motion in perpendicularly magnetized materials, Nat. Commun. 3 (2012) 847.
[10] J.H. Franken, Y. Yin, A.J. Schellekens, A. van den Brink, H.J.M. Swagten, B. Koopmans, Voltage-gated pinning in a magnetic domain-wall conduit, Appl. Phys. Lett. 103 (2013) 102411.
[11] U. Bauer, L. Yao, A.J. Tan, P. Agrawal, S. Emori, H.L. Tuller, S. van Dijken, G.S.D. Beach, Magneto-ionic control of interfacial magnetism, Nat. Mater. 14 (2015) 174–181.
[12] Y.T. Liu, S. Ono, G. Agnus, J.P. Adam, S. Jaiswal, J. Langer, B. Ocker, D. Ravelosona, L. Herrera Diez, Electric field controlled domain wall dynamics and magnetic easy axis switching in liquid gated CoFeB/MgO films, J. Appl. Phys. 122 (2017) 133907.
[13] K.J.A. Franke, B. Van de Wiele, Y. Shirahata, S.J. Hamalainen, T. Taniyama, S. van Dijken, Reversible electric-field-driven magnetic domain-wall motion, Phys. Rev. X 5 (2015) 011010.
[14] T.H.E. Lahtinen, J.O. Tuomi, S. van Dijken, Pattern transfer and electric-field-induced magnetic domain formation in multiferroic heterostructures, Adv. Mater. 23 (2011) 3187–3191.
[15] P. Li, Y. Zhao, S. Zhang, A. Chen, D. Li, J. Ma, Y. Liu, D.T. Pierce, J. Unguris, H.G. Piao, H. Zhang, M. Zhu, X. Zhang, X. Han, M. Pan, C.W. Nan, Spatially resolved ferroelectric domain-switching-controlled magnetism in $Co_{40}Fe_{40}B_{20}$/Pb($Mg_{1/3}Nb_{2/3}$)$_{0.7}Ti_{0.3}O_3$ multiferroic heterostructure, ACS Appl. Mater. Interfaces 9 (2017) 2642–2649.
[16] N. Lei, T. Devolder, G. Agnus, P. Aubert, L. Daniel, J.V. Kim, W.S. Zhao, T. Trypiniotis, R.P. Cowburn, C. Chappert, D. Ravelosona, P. Lecoeur, Strain-controlled magnetic domain wall propagation in hybrid piezoelectric/ferromagnetic structures, Nat. Commun. 4 (2013) 1378.
[17] E. Mikheev, I. Stolichnov, E. De Ranieri, J. Wunderlich, H.J. Trodahl, A.W. Rushforth, S.W.E. Riester, R.P. Campion, K.W. Edmonds, B.L. Gallagher, N. Setter, Magnetic domain wall propagation under ferroelectric control, Phys. Rev. B 86 (2012) 235130.
[18] J.-J. Wang, T.-N. Yang, J.A. Zorn, E. Wang, J. Irwin, S. Lindemann, M.S. Rzchowski, J.-M. Hu, C.-B. Eom, L.-Q. Chen, Strain anisotropy and magnetic domain structures in multiferroic heterostructures: high-throughput finite-element and phase-field studies, Acta Mater. 176 (2019) 73–83.
[19] W. Eerenstein, M. Wiora, J.L. Prieto, J.F. Scott, N.D. Mathur, Giant sharp and persistent converse magnetoelectric effects in multiferroic epitaxial heterostructures, Nat. Mater. 6 (2007) 348–351.
[20] H.-J. Kim, M.-S. Jung, C.-Y. You, J.-I. Hong, Controllable magnetic anisotropy of ferromagnet/antiferromagnet bilayers coupled with piezoelectric strain, Acta Mater. 171 (2019) 170–175.

[21] C.G. Duan, J.P. Velev, R.F. Sabirianov, Z.Q. Zhu, J.H. Chu, S.S. Jaswal, E.Y. Tsymbal, Surface magnetoelectric effect in ferromagnetic metal films, Phys. Rev. Lett. 101 (2008) 137201.
[22] J.T. Heron, J.L. Bosse, Q. He, Y. Gao, M. Trassin, L. Ye, J.D. Clarkson, C. Wang, J. Liu, S. Salahuddin, D.C. Ralph, D.G. Schlom, J. Iniguez, B.D. Huey, R. Ramesh, Deterministic switching of ferromagnetism at room temperature using an electric field, Nature 516 (2014) 370–373.
[23] H.B. Li, N.P. Lu, Q.H. Zhang, Y.J. Wang, D.Q. Feng, T.Z. Chen, S.Z. Yang, Z. Duan, Z.L. Li, Y.J. Shi, W.C. Wang, W.H. Wang, K. Jin, H. Liu, J. Ma, L. Gu, C.W. Nan, P. Yu, Electric-field control of ferromagnetism through oxygen ion gating, Nat. Commun. 8 (2017) 2156.
[24] T. Maruyama, Y. Shiota, T. Nozaki, K. Ohta, N. Toda, M. Mizuguchi, A.A. Tulapurkar, T. Shinjo, M. Shiraishi, S. Mizukami, Y. Ando, Y. Suzuki, Large voltage-induced magnetic anisotropy change in a few atomic layers of iron, Nat. Nanotech. 4 (2009) 158–161.
[25] Y. Ba, Y. Liu, P. Li, L. Wu, J. Unguris, D.T. Pierce, D. Yang, C. Feng, Y. Zhang, H. Wu, D. Li, Y. Chang, J. Zhang, X. Han, J. Cai, C.-W. Nan, Y. Zhao, Spatially resolved electric-field manipulation of magnetism for CoFeB mesoscopic discs on ferroelectrics, Adv. Funct. Mater. 28 (2018) 1706448.
[26] J. Yao, X. Song, X. Gao, G. Tian, P. Li, H. Fan, Z. Huang, W. Yang, D. Chen, Z. Fan, M. Zeng, J.M. Liu, Electrically driven reversible magnetic rotation in nanoscale multiferroic heterostructures, ACS Nano 12 (2018) 6767–6776.
[27] X. Song, X.S. Gao, L.J. M., Electric field driven magnetic switching in nanoscale multiferroic heterostructures, Acta Phys. Sin. 67 (2018) 157512.
[28] A. Chen, Y. Zhao, P. Li, X. Zhang, R. Peng, H. Huang, L. Zou, X. Zheng, S. Zhang, P. Miao, Y. Lu, J. Cai, C.W. Nan, Angular dependence of exchange bias and magnetization reversal controlled by electric-field-induced competing anisotropies, Adv. Mater. 28 (2016) 363–369.
[29] M. Ghidini, R. Mansell, F. Maccherozzi, X. Moya, L.C. Phillips, W. Yan, D. Pesquera, C.H.W. Barnes, R.P. Cowburn, J.-M. Hu, S.S. Dhesi, N.D. Mathur, Shear-strain-mediated magnetoelectric effects revealed by imaging, Nat. Mater. 18 (2019) 840–845.
[30] I.V. Soldatov, R. Schäfer, Advances in quantitative Kerr microscopy, Phys. Rev. B 95 (2017) 014426.
[31] J.X. Zhang, L.Q. Chen, Phase-field microelasticity theory and micromagnetic simulations of domain structures in giant magnetostrictive materials, Acta Mater. 53 (2005) 2845–2855.
[32] R.C. Peng, J.M. Hu, L.Q. Chen, C.W. Nan, On the speed of piezostrain-mediated voltage-driven perpendicular magnetization reversal: a computational elasto-dynamics-micromagnetic phase-field study, NPG Asia Mater. 9 (2017) e404.
[33] M. Frommberger, S. Glasmachers, C. Schmutz, J. McCord, E. Quandt, Microscopic magnetic and high-frequency properties of a stress sensor using FeCoBSi magnetostrictive thin films, IEEE Trans. Magn. 41 (2005) 3691–3693.
[34] E. Lage, C. Kirchhof, V. Hrkac, L. Kienle, R. Jahns, R. Knochel, E. Quandt, D. Meyners, Exchange biasing of magnetoelectric composites, Nat. Mater. 11 (2012) 523–529.
[35] R.C. Wetherhold, V.H. Guerrero, Magnetoelastic interaction in magneto strictive spring-magnet multilayers, J. Magn. Magn. Mater. 269 (2004) 61–69.
[36] A. Zhukov, M. Ipatov, M. Churyukanova, S. Kaloshkin, V. Zhukova, Giant magnetoimpedance in thin amorphous wires: From manipulation of magnetic field dependence to industrial applications, J. Alloy. Compd. 586 (2014) S279–S286.
[37] L. Zhang, W.B. Zhu, H.Y. Zheng, X. Wang, M. Bi, N. Wang, P.H. Zhou, H.P. Lu, J.L. Xie, L.J. Deng, Thickness-dependent magnetic properties of patterned Fe-CoBSi amorphous thin films on silicon substrate, IEEE Trans. Magn. 51 (2015) 2003504.
[38] D. La-Orauttapong, B. Noheda, Z.G. Ye, P.M. Gehring, J. Toulouse, D.E. Cox, G. Shirane, Phase diagram of the relaxor ferroelectric (1-x)$Pb(Zn_{1/3}Nb_{2/3})O_3$-x$PbTiO_3$, Phys. Rev. B 65 (2002) 144101.
[39] M. Liu, B.M. Howe, L. Grazulis, K. Mahalingam, T.X. Nan, N.X. Sun, G.J. Brown, Voltage-impulse-induced non-volatile ferroelastic switching of ferromagnetic resonance for reconfigurable magnetoelectric microwave devices, Adv. Mater. 25 (2013) 4886–4892.
[40] M. Liu, T. Nan, J.-M. Hu, S. Zhao, Z. Zhou, C. Wang, Z.-D. Jiang, W. Ren, Z.-G. Ye, L.-Q. Chen, N.X. Sun, Electrically controlled non-volatile switching of magnetism in multiferroic heterostructures via engineered ferroelastic domain states, NPG Asia Mater. 8 (2016) e316.
[41] R. Lo Conte, Z. Xiao, C. Chen, C.V. Stan, J. Gorchon, A. El-Ghazaly, M.E. Nowakowski, H. Sohn, A. Pattabi, A. Scholl, N. Tamura, A. Sepulveda, G.P. Carman, R.N. Candler, J. Bokor, Influence of nonuniform micron-scale strain distributions on the electrical reorientation of magnetic microstructures in a composite multiferroic heterostructure, Nano Lett. 18 (2018) 1952–1961.
[42] A. Chen, Y. Wen, B. Fang, Y. Zhao, Q. Zhang, Y. Chang, P. Li, H. Wu, H. Huang, Y. Lu, Z. Zeng, J. Cai, X. Han, T. Wu, X.X. Zhang, Y. Zhao, Giant nonvolatile manipulation of magnetoresistance in magnetic tunnel junctions by electric fields via magnetoelectric coupling, Nat. Commun. 10 (2019) 243.
[43] T. Wu, A. Bur, P. Zhao, K.P. Mohanchandra, K. Wong, K.L. Wang, C.S. Lynch, G.P. Carman, Giant electric-field-induced reversible and permanent magnetization reorientation on magnetoelectric Ni/(011) $[Pb(Mg_{1/3}Nb_{2/3})O_3]_{(1-x)}$-$[PbTiO_3]_x$ heterostructure, Appl. Phys. Lett. 98 (2011) 012504.